Effect of degraded environmental conditions on the service behavior of a X65 pipeline steel not designed for hydrogen transport

C. Mendibide, F. Vucko, M. Martinez, G.R. Joshi, J. Kittel

▶ **To cite this version:**

C. Mendibide, F. Vucko, M. Martinez, G.R. Joshi, J. Kittel. Effect of degraded environmental conditions on the service behavior of a X65 pipeline steel not designed for hydrogen transport. International Journal of Hydrogen Energy, 2024, 52 (Part A), pp.1019-1032. 10.1016/j.ijhydene.2023.05.309 . hal-04431257

HAL Id: hal-04431257
https://ifp.hal.science/hal-04431257

Submitted on 1 Feb 2024

HAL is a multi-disciplinary open access archive for the deposit and dissemination of scientific research documents, whether they are published or not. The documents may come from teaching and research institutions in France or abroad, or from public or private research centers.

L'archive ouverte pluridisciplinaire **HAL**, est destinée au dépôt et à la diffusion de documents scientifiques de niveau recherche, publiés ou non, émanant des établissements d'enseignement et de recherche français ou étrangers, des laboratoires publics ou privés.

Distributed under a Creative Commons Attribution - NonCommercial - NoDerivatives 4.0 International License

Available online at www.sciencedirect.com

ScienceDirect

journal homepage: www.elsevier.com/locate/he

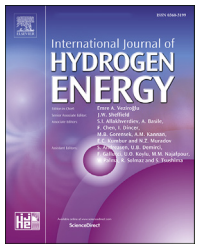

Effect of degraded environmental conditions on the service behavior of a X65 pipeline steel not designed for hydrogen transport

C. Mendibide [a,*], F. Vucko [a], M. Martinez [b], G.R. Joshi [b], J. Kittel [b]

[a] Institut de La Corrosion (French Corrosion Institute), Part of RISE - ZA Du Parc, Secteur Gampille, F-42490, Fraisses, France

[b] IFP Energies Nouvelles, Rond-point de L'échangeur de Solaize, BP3 - 69360, Solaize, France

HIGHLIGHTS

- The risk of hydrogen assisted cracking is low with ×65 up to 100 bar H_2 in the absence of gas contaminants.
- The decrease in fracture toughness is minimal under dry H_2 even though some embrittlement is visible in the fractured surface.
- The fracture toughness in gaseous H_2 significantly decreases in presence of humidity with traces of H_2S.
- The extent of hydrogen induced cracking, even in the in presence of humid H_2S contamination, remains low.
- The hydrogen ingress assessed through TDS measurement was extremely low.

ARTICLE INFO

Article history:
Received 18 October 2022
Received in revised form
16 May 2023
Accepted 29 May 2023
Available online 15 June 2023

Keywords:
Hydrogen transport
Pipeline
Fracture toughness
Slow strain rate test
Hydrogen induced cracking
Hydrogen permeation

ABSTRACT

With the international drive to deploy green energies and decarbonized intermediates in the place of fossil fuel sources, a large number of developed countries are actively preparing for a future where hydrogen plays a strategic role as an energy storage medium. Producing and using hydrogen requires the rapid expansion of a dedicated, economically viable industrial sector. Nevertheless, questions on how to safely store, transport and distribute hydrogen remain an important priority today. In countries with existing natural gas transport grids, the possibility to retrofit these networks to store and transport hydrogen-natural gas blends is being studied.

A key challenge is to evaluate how pressurized H_2 would interact with steel structures with regards structural embrittlement of the latter, with a view to exploiting existing transport infrastructures for storage and transport applications. In this work, we evaluate the H_2-performance of a non-hydrogen service ×65 pipeline steel. The cracking susceptibility of this steel grade has been evaluated at 100 bar H_2 using slow strain rate testing, Constant strain testing and fracture toughness measurements. Accompanying hydrogen permeation tests under pressure provide diffusion data and elucidate the discussion. Exposures were carried out in dry or wet H_2 and with or without H_2S contamination at levels representative of biogas. The results underline that the impact of dry or wet hydrogen on this grade are moderate. The presence of traces of H_2S together with humidity could risk seriously degrading the mechanical performance of the ×65 steel grade.

* *Corresponding author.*
E-mail address: christophe.mendibide@institut-corrosion.fr (C. Mendibide).

https://doi.org/10.1016/j.ijhydene.2023.05.309

0360-3199/© 2023 The Authors. Published by Elsevier Ltd on behalf of Hydrogen Energy Publications LLC. This is an open access article under the CC BY-NC-ND license (http://creativecommons.org/licenses/by-nc-nd/4.0/).

© 2023 The Authors. Published by Elsevier Ltd on behalf of Hydrogen Energy Publications LLC. This is an open access article under the CC BY-NC-ND license (http://creativecommons.org/licenses/by-nc-nd/4.0/).

Introduction

With the international drive to decrease dependance of fossil energies and the imminent requirement to develop green alternatives and clean intermediates, hydrogen appears to be one of the most promising power sources in the near future. By 2050, hydrogen – through conversion to electricity via a fuel cell, as a feed source to produce synthetic natural gas or through direct combustion - intends to cover between 8 and 24% of the European energy demand [1]. The development of H_2 energy will however need the construction and ramp-up of dedicated industrial sectors, including steam reforming and electrolysis plants, through the development of efficient electrolysers, fuel cells, catalysts or chemicals crackers, safe transport and storage sites, safe vehicles and development of H_2 refueling station networks in the different European countries [2,3].

From a material qualification standpoint, several questions are raised considering that hydrogen can be easily absorbed by metallic alloys with well-known risk of embrittlement and premature failure through modifications to the fracture toughness/strains to failure if service conditions are not controlled [4,5]. This risk is on the forefront of preoccupations related to the safe retrofitting of the existing natural gas transport grids for hydrogen transport and to hydrogen blending in natural gas [6,7].

Previous work indicates that blending natural gas with hydrogen is possible up to limited levels [8,9]. For instance, the injection of H_2 into natural gas networks is already carried out today at blends up to 10% H_2 in certain European nations [10], and plans are in place to increase this concentration. Crucially, moving to higher hydrogen/natural gas blends warrants further understanding on the hydrogen – material response, through qualification and risk assessments. Several questions remain unanswered on the suitability of using ferritic steel to transport H_2 blends, since this gas is recognized as an agent (once absorbed) that leads to embrittlement and premature component failure [11–13].

Another material integrity challenge relates to underground storage [14,15], where hydrogen could be humid (either liquid water or water vapor) in the presence of impurities such as H_2S or oxygen gas. Both contaminants are indeed present in biomethane, up to some hundreds of parts per million (ppm) each [16], depending on the feedstock considered. At least for storage applications, H_2S can also come from microbial activity and therefore may reach higher contents, constituting therefore a corrosive and potentially more hydrogenating environment.

For a risk assessment approach, several types of hydrogen assisted failure should be considered. The first is hydrogen induced cracking (HIC) or stress oriented induced cracking (SOHIC) which are well-known type of cracking in the petroleum production and refining sectors when H_2S is present in the environment. Brittle cracking of low-alloyed steel can occur when diffusible hydrogen accumulates at microstructural singularities (inclusions, segregation, dislocations …) and recombines in a gaseous form. Some research results underline that the threshold content of diffusible hydrogen for cracking in ×65 pipeline steel is about 1 ppm [17], although this can vary depending on the microstructure state and the rate of hydrogen uptake. Under dry pressurized hydrogen, in transport and storage application, it is suggested that such high levels cannot be reached in pipeline steel grades [18]. However, diffusible hydrogen contents close to 1 ppm have been measured in cold-worked specimen exposed to condition simulating hydrogen transport [19]. This observation may underline a risk of HIC failure even under dry H_2 pressure in the case of uncontrolled maintenance operations or at pipelines irregularities like welds.

Considering the retrofitting of natural gas steel pipeline network, the possible impact of the use of aged pipeline material having been operated for years with only methane is also a relevant parameter since decades of operations can affect the mechanical properties [20].

Odorant compounds are generally added to natural gas and the use of ductile material ensures non-brittle cracking; the detection of odorant smells indicates leaks that may be repaired. Hydrogen, however, is difficult to contain and may present frequent leaking issues. A possible adverse impact of hydrogen once employed in retrofitted networks is indeed the risk of toughness loss of the pipeline steel. Considering the well-known risk of embrittlement and associated loss of toughness generated by hydrogen ingress in the material structure, dramatic brittle pipeline failures is possible if the material loses ductility and/or decreases its fracture toughness. This has been demonstrated particularly true with aged pipeline steel materials [21,22]. This loss of ductility can be evaluated through slow strain rate test (SSRT) on smooth or notched specimens to evaluate the effect of hydrogen blending on the crack initiation susceptibility [23–25], and by evaluating the resistance to crack propagation through different standardized techniques that can be adapted to testing under H_2 pressure. Some of these techniques are specified in existing ASME documents [26,27]. Their application to evaluate pipeline steels suffer, however, from certain limitations due to the very high ductility of the material that prevent establishing the validity checks specified in the standards.

Some published works [23,28] also show, that the value of the stress intensity factor under hydrogen (K_{IH}, $MPa.m^{1/2}$) strongly depends on the stress application mode (i.e. constant displacement or constant stress). This is particularly important for steels with the low yield strengths which corresponds to pipeline steels. Both works prove the limitation of the tests using constant strain to determine the K_{IH} for line pipe steel. This K_{IH}, also sometimes referred to as the steel fracture toughness under hydrogen, of standard low-grade pipeline steels remains generally sufficiently high under typical transport and distribution pressures [29–36] but can be critical for high grades [29,37].

Table 1 – Composition of the tested steel in %wt determined by optical emission spectroscopy compared with the minimum requirement for the levels PSL1 and PSL 2 from API 5 L.

	C	Si	Mn	P	S	Nb Ti V	N	CEPcm
Requ. PSL1	0.26 max		1.45 max	0.03 max	0.03 max	0.15 max		
Requ. PSL2	0.12 max	0.45 max	1.85 max	0.02 max	0.01 max	0.15 max		0.25 max
Actual	0.052	0.031	1.53	0.01	<0.001	Nb + Ti + V = 0.055	0.003	0.15

Table 2 – : Mechanical properties of the tested steel compared with the minimum requirement for the levels PSL1 and PSL 2 from API 5 L. $\sigma_{y,\ 0.2\%}$ (MPa) = yield strength 0.2%, $\sigma_{y,\ 0.5\%}$ (MPa) = yield strength 0.5%, σ_{UTS} (MPa) – ultimate tensile strength, E_f (%) = elongation to failure (%), RA (%) = percent reduction in cross-sectional area of tensile sample after fracture ((initial area – final area)/(initial area) × 100).

	$\sigma_{y,\ 0.2\%}$ (MPa)	$\sigma_{y,\ 0.5\%}$ (MPa)	σ_{UTS} (MPa)	$\sigma_{y,\ 0.5\%}$/UTS	E_f(%)	RA (%)	Core Hardness (HV10kg)
Req. PSL1	n/a	450 max	535 min	n/a	n/a	n/a	
Req. PSL2	n/a	450–600	535–760	0.93 max	16 min	n/a	
Actual	532	537	608	0.88	21.5	85	205

From a literature standpoint, the decrease of the fatigue resistance of low alloyed steel under dry hydrogen has clearly been established with an impact on the crack initiation (the number of cycles necessary to initiate a crack is lower under hydrogen) [38] and propagation (the propagation rate can be higher under hydrogen) [39]. From several references [40–47], it seems however that the resistance to fatigue under hydrogen pressure is strongly dependant on the loading conditions. Under a threshold amplitude, no effect of hydrogen is observed up to very high partial pressures (100 bar and higher) whereas, if an amplitude threshold is reached, a dramatic decrease of the resistance is observed. This conclusion was corroborated by fatigue tests conducted in the frame of a European project completed to address the risk of blending natural gas with hydrogen [48,49]. This project underlined that, for an operating pressure of 67 bar, no effect of hydrogen up to a blend level of 100% is observed if a ×52 steel grade is fatigue loaded under an amplitude of 7.3 MPa $\sqrt{m}$. On the contrary, with an amplitude of 11.3 MPa$\sqrt{m}$, an effect of hydrogen is highlighted for a blend level as low as 20%. In the same project, a lower fatigue resistance in presence of hydrogen was highlighted on "vintage" structure (pipelines having been operated for years under natural gas) underlining a possible increased risk of failure in case of retrofitting application. In transport applications, if a risk of fatigue failures is clearly established from the literature, it seems therefore that it could be mitigated by a strict control of the in-service loading conditions.

To contribute to the growing body of work in this domain, our study focuses on the characterization of the effect of hydrogen up to a partial pressure of 100 bar on the service properties of an ×65 pipeline steel. The objective is to evaluate the risk of hydrogen-induced mechanical failure, in the presence of humidity or H_2S traces, of a steel material that is not specifically designed for operation under hydrogen.

Materials and methods

Material

The material selected for this work was a ×65 seam welded pipeline steel produced according to a thermomechanical controlled process. The composition of the selected grade is given in Table 1 and its mechanical properties in Table 2.

The selected grade is appropriate for oil & gas application but not designed for sour service because it can suffer from hydrogen induced cracking in the presence of H_2S. Indeed, ensuring that hydrogen assisted failures of this grade could be observed if the test conditions are critical was the primary reason for the selection of this grade for the study. The grade complies with the PSL2 level specified in the API 5 L construction code [50].

The grade has a ferritic microstructure with pearlite at grain boundaries (Fig. 1). No macro-segregations are visible after nital etching (2% nitric acid in ethanol).

Standard HIC tests

To check if the material considered in the study was susceptible to cracking, standard HIC tests were first conducted according to NACE TM0284 [51]. The results were analyzed by determining the different crack-length ratio through metallographic cross-sections after first conducting ultrasonic inspections to observe HIC indications.

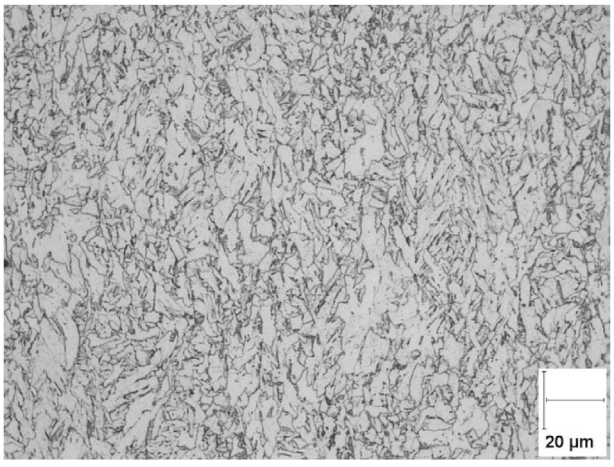

Fig. 1 – Microstructure of the studied ×65 steel after Nital Etching.

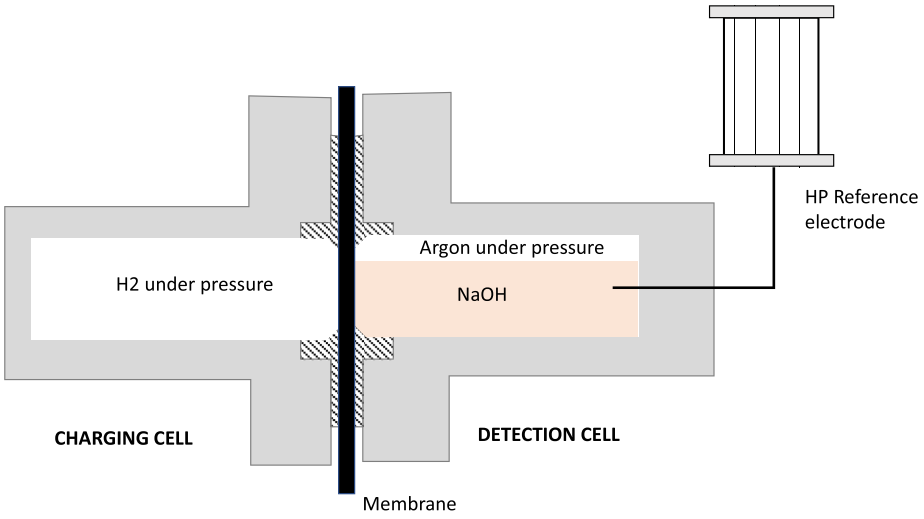

Fig. 2 – Schematic of the electrochemical H-permeation Devanathan-Stachurski cell.

The sampling and preparation of the specimens ($20 \times 12 \times 100$ mm^3 cuboid) were performed as per standard practices. The HIC specimens were machined using milling with the 2 last final machining passes removing not more than 25 μm of material each. After machining the average roughness was lower than 0.8 μm. The specimens were then polished with a P320 SiC grit and degreased before testing.

The following test procedure was applied.

- Deaeration of the test solution (NACE A, 0.5% acetic acid in 50 g/L NaCl) in a separate preparation reservoir with argon bubbling at a flow rate higher than 100 mL/min. In this step, the test cell containing the specimens is connected to the reservoir outlet to be deaerated simultaneously;
- Transfer of the solution to the cell from the reservoir under gas pressure;
- Continuous deaeration in the cell with dissolved oxygen measurement;
- Saturation of the solution with 100% H_2S if $[O_2] < 10$ ppb;
- Exposure for 4 days.
- *Ex situ* evaluation of HIC

Hydrogen permeation test

Hydrogen diffusion through a metal membrane is traditionally studied by employing a Devanathan-Stachurski (DS) type permeation cell [52]. This technique was used to perform permeation test under pressure. The cell comprises two independent compartments, that can hold a volume of solution or a pressurized gas, that clamp and secure in place a metal membrane (the ×65 steel) between them. One of the compartments is the hydrogen charging cell whereas the other serves as the anodic or oxidation cell (containing 0.1 M NaOH liquid solution). In the charging cell, hydrogen is adsorbed and absorbed ×65 steel surface under the pressure of the studied test gas. A quasi-equilibrium between adsorbed and absorbed hydrogen is established at this "entry" surface and atomic hydrogen diffuses across the membrane thickness under a diffusion gradient to the other, "exit" oxidation face. Through the application of an anodic potential vs. the reference electrode at this exit surface of the alloy membrane, the diffusing hydrogen is oxidized, and the corresponding current is measured through the counter electrode. The evolution of this oxidation current is informative on hydrogen diffusion across the alloy, and serves to evaluate the uptake of hydrogen, its diffusivity, and retention within the alloy under question.

A schematic of the cell is shown in Fig. 2.

This double compartment cell permits us to impose a high pressure on a single metallic membrane (exposed area = 2.85 cm^2/Thickness 2 mm). The hydrogen charging (left) and anodic oxidation (right) cells can hold a volume of 70 mL, and a potentiostat is used to measure the hydrogen oxidation current.

Practically, the detection cell is equipped with an external Ag/AgCl reference electrode capable of operating under pressure. The anodic detection cell is also pressurized to avoid/minimize a plastic deformation of the membrane under hydrogen pressure from the opposite compartment. The membrane is used as the working electrode and the metallic detection cell as the counter electrode.

Three test conditions were considered.

- 1) *Dry hydrogen:* the charging cell was pressurized under 100 bar of dry hydrogen using a commercial cylinder of high purity. To ensure that the gas was dry in the experiments, some desiccant crystals were added in the charging cell.
- 2) *Wet hydrogen:* the charging cell was pressurized under 100 bar under 100 bar H_2 but a small volume of demineralized water was introduced in the charging cell before pressurizing with the test gas. This water humidifies the gas but was not in contact with the test specimen during the exposures. According to the test temperature considered (around 25 °C), the water vapor pressure in these selected test conditions is 33 mbar. Considering the ideal gas law, this level of partial pressure corresponds to not more that 10^{-4} mol of water. Therefore if at least this quantity of water is introduced in a closed vessel, i.e. a

volume of 18 μL in our experimental device, water saturation is achieved in the gas phase. Considering this analysis and the fact that traces of water are enough to saturate the gas phase with water vapor, we can consider that each experiment was conducted under 100 bar H_2 and more than 90% of relative humidity.

- 3) *Wet hydrogen + H_2S:* the charging cell was pressurized under 100 bar of humid hydrogen with 1000 ppm of H_2S to simulate a contamination. This value corresponds to a maximum level that can be present as a residual contaminant in biogas. For testing purposes, 99 bar of pure hydrogen was introduced in the vessel and made up to 100 bar with an "Argon +10%H_2S" gas mixture. In this condition, the corresponding partial pressures were 99 bar of humid H_2, 1 mbar of H_2S and 9 mbar of Argon.

The following test protocol was employed. The membrane was first polished to 1200-grit SiC paper. The membrane is then set-up in the permeation cell before completing a leak test with pressurized helium. The exit surface of the membrane is then pickled in concentrated inhibited HCl inhibited with hexamethylenetetramine (corrosion inhibitor) and then coated with palladium. This coating is applied through electrodeposition using a solution containing 5 g/L of $PdCl_2$ in ammonia 28% under a galvanostatic polarization at −2 mA/cm^2 for 90 s. After rinsing with demineralized water, the 0.1 M NaOH solution used for electrochemical extraction is introduced in the detection side and the cell is pressurized to 50 bar using Argon. This pressure is just below the maximum operating pressure of the reference electrode. The membrane is then polarized to +100 mV/Ag/AgCl until a background current density not higher that some tens of nA/cm^2 is measured. The charging cell is then vacuumed using a pump and loaded at 100 bar with the gas of interest (100%H_2 or "99% H_2 + 0.9% Ar + 0.1% H_2S") and the permeation flux monitored. In all experiments, the detection cell was pressurized at 50 bar which ensured that any deformation of the membrane by pressurization of the charging cell remains in the elastic range of the tested material. The increase in pressure was completed "step-by-step" in both cells to equilibrate the pressures during experiment start. Subsequently, hydrogen oxidation current was tracked over 150 h.

Hydrogen induced cracking (HIC) tests

The hydrogen induced cracking experiments were conducted in a standard autoclave using a similar protocol as the one selected for permeation. The test specimens were first introduced in the vessel before leak testing with several cycles of pressurization release using Helium. The vessel was then pressurized with the test gas for 1 month.

The specimens considered in each experiment were loaded using a 4-point bend jig. The applied load in each case was 100% of the actual yield strength of the base metal measured by standard mechanical tests. All specimens were sampled in the longitudinal direction of a pipe section at mid-thickness. In all experiments 2 specimens were tested. The first sampled in the base metal and the second through the girth weld of the pipe.

After the period of exposure, the specimens were carefully observed using an optical microscope to highlight crack initiations and ultrasonic inspected for internal cracking.

In all experiment non-loaded test coupons were also introduced in the autoclave for thermal desorption spectroscopy analysis (TDS) after exposures. After each test, these coupons were immersed in liquid nitrogen to avoid hydrogen effusion until the TDS experiments were started. The hydrogen content was measured using a Bruker G8 Galileo analyzer (Thermal conductivity detection). The quantitative analysis of hydrogen content was carried out by heating the samples up to 950 °C in a flow of pure nitrogen gas, using a constant heating rate of 0.33, 1 and 2 °C/s. Calibration of the instrument was performed using helium gas. The filters (molecular sieve, Schütze reagent and activated carbon) were changed prior to calibration and measurements.

Slow strain rate tensile tests (SSRT)

Published data on ×80 pipeline steel underline that embrittlement can be observed on smooth tensile specimens [25,53]. On this basis, and to evaluate the susceptibility of the material to crack initiation, slow strain rate tests were conducted on smooth tensile samples machined in the longitudinal direction. A slow strain rate test bench was set-up with an autoclave containing a tensile specimen. The same start-up procedure as the one described in section Hydrogen induced cracking (HIC) tests was considered. After pressurizing the autoclave with the gas, the specimen was loaded to failure at a fixed extension rate of 10^{-6} inch s^{-1}. In all experiments, a NACE subsize specimen machined as per the schematic in Fig. 3 was used.

This specimen has a gauge length of 1 inch leading to a strain rate of 10^{-6} s^{-1} after reaching the yield point. The material properties were compared to a reference test conducted under 100 bar of Helium. Only the base material was tested using SSRT.

Incremental step loading – fracture toughness evaluation

To evaluate the amount of stress required to propagate an existing crack/flaw in the different H_2 environments (fracture toughness), incremental or rising step loading (RSL) tests were

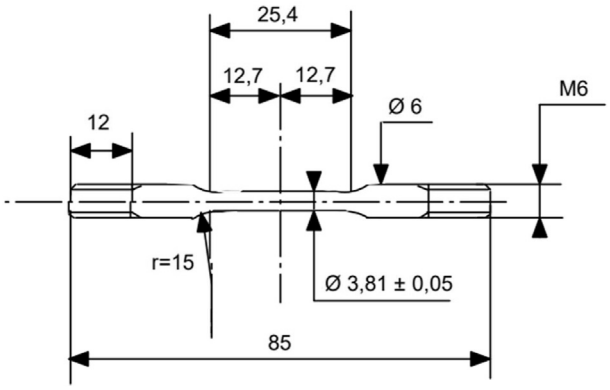

Fig. 3 – Schematic of the specimen used in the SSRT experiments (dimensions in mm).

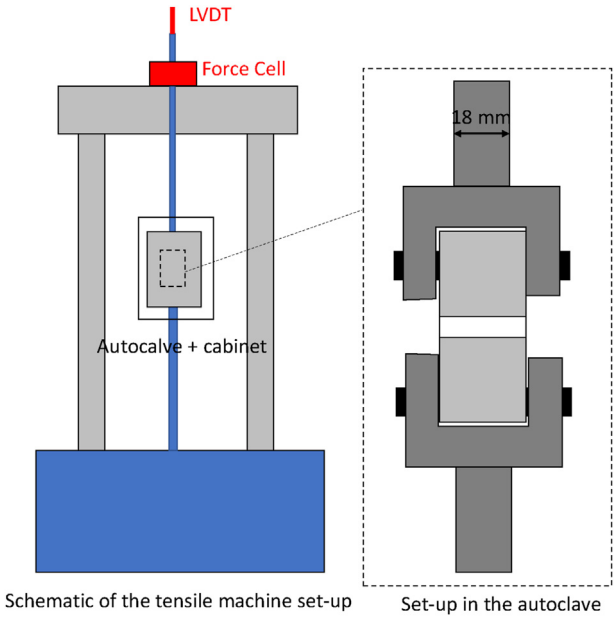

Fig. 4 – Schematic presentation of the test set-up for fracture toughness evaluation.

conducted. For each test, the specimens were set-up in an autoclave fixed on a tensile machine as schematically presented in Fig. 4. A displacement and force monitoring are ensured at the top of the loading line using calibrated linear variable differential transformer (LVDT) sensor and force cells (outside the autoclave). The autoclave is placed in a sealed polycarbonate cabinet flushed with nitrogen during the test to avoid hydrogen ignition during the loading in case of leak.

The crack initiation was checked using electric crack growth monitoring (ECGM), as detailed further below, and variations in the crosshead displacement under the constant force steps.

The compact tension (CT) specimens selected for the experiments were chosen according to the pipeline wall thickness limitation. The maximum possible CT size was 15 mm in thickness and 30 mm in width (B15W30) as shown at Fig. 5, with.

- B = 15 mm
- W = 30 mm
- Wt = 39 mm
- Lt = 36 mm
- L = 16.5 mm

Prior to testing, the specimens were pre-cracked in fatigue with a target of initial crack length (a_0) of 15 mm.

RSL tests were done on a 100 kN tensile machine programmed to track the rising load sequence. The specimens were also equipped with 4 stainless-steel wires laser-welded on the face, to monitor crack propagation through ECGM (Electric Crack Growth Monitoring using the alternating current potential drop (ACPD) approach). Two of these wires were used to apply a low frequency alternative current (AC), and the others allowed to measure a potential to estimate the resistance of the specimen. The wires were protected with a Teflon sheath and a varnish layer to reinforce the welds.

From the schematic of the specimen presented in Fig. 5, the electrical resistance of the specimen is expressed as

$$R = \rho \frac{L}{S} \tag{1}$$

with $S = B \times (W - a)$ the section, L the length and ρ the electrical resistivity (xx ohm) of the material

Considering R_0 the initial resistance of the specimen and R(t) the resistance monitored during the test, we obtain:

$$\frac{R}{R_0} = \frac{W - a_0}{W - a} \tag{2}$$

with a_0 the initial crack length after pre-cracking in fatigue.

During each test, it is therefore possible to calculate the crack length a (mm) as a function of the measured resistance as:

$$a(t) = W - \left(\frac{R_0}{R(t)}(W - a_0)\right) \tag{3}$$

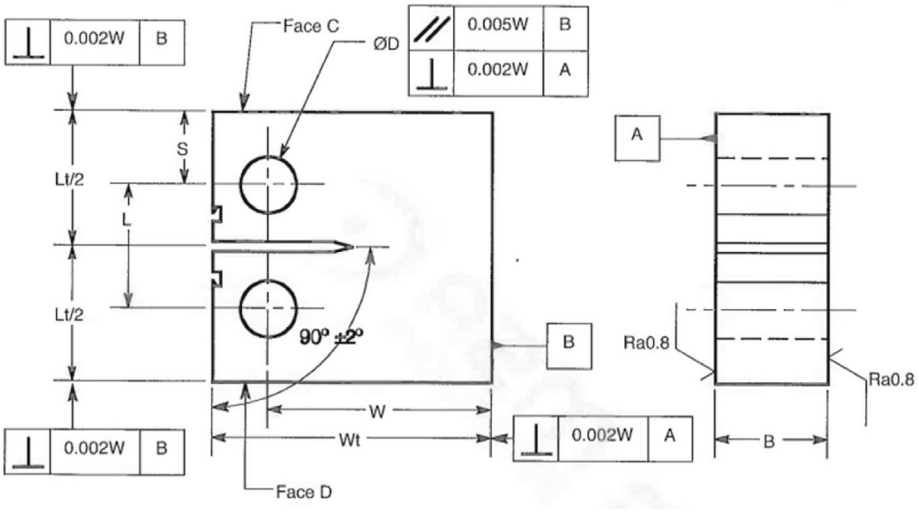

Fig. 5 – Sketch of a standard CT B15/W30 specimen.

The fracture toughness of the material was then estimated through a post treatment of the data considering the force level at which the crack starts to initiate and not only the force at fracture.

The same start-up procedure defined for SSRT was used. Once the autoclave was pressurized, the specimens were submitted to a loading sequence consisting of 10 loading stages of 2 h and 10 loading stages of 4 h with each load increment corresponding to 5% of the air fracture toughness expected for the pipeline material considered. Since the force sensor was outside the autoclave, the force at failure was systematically corrected for the effect of pressure on the loading line measured at the pressurization stage.

After testing, the force step at which the crack propagation is detected from ECGM was used to calculate K_{IH} according to the formula in Equation (4) from ASTM F1681. To estimate the threshold force, the evolution of the variation of the loading line is also used and cross-checked with the resistance measurement, to estimate the threshold stress. Indeed, since the load is under force control and the displacement of the line is measured, the initiation of the crack propagation can lead to slight increases in the displacement monitoring.

$$K = \left[\frac{P}{B.W^{\frac{1}{2}}}\right] f\left(\frac{a_0}{W}\right) \tag{4}$$

Where

$$f\left(\frac{a_0}{W}\right) = \frac{2+\frac{a_0}{W}}{\left(1-\frac{a_0}{W}\right)^{\frac{3}{2}}}\left[0.886 + 4.64\left(\frac{a_0}{W}\right) - 13.32\left(\frac{a_0}{W}\right)^2 + 14.72\left(\frac{a_0}{W}\right)^3 - 5.6\left(\frac{a_0}{W}\right)^4\right] \tag{5}$$

With.

- a_0 the initial crack length measured through fractographic observations considering a minimum of 5 measurements.
- B, W, the dimensions of the CT specimen used (see Fig. 5)
- P the force at failure.

Considering that some ductility is observed in the fracture of the specimens and that the geometrical validity requirement of the ASTM F1681 cannot be met due to pipeline size limitation, the K_{IH} values calculated should be considered only in relative manner to assess the effect of the environment. Only the specimen tested with H_2S met all the standard requirements leading to an accurate evaluation of the fracture toughness. According to a preliminary work not presented in this paper, all K_{IH} values higher than 60–70 MPa$\sqrt{m}$ are affected by plasticity and probably underestimated. This issue is also expected to be encountered if the crack arrest test method described for H_2 service qualification of pipeline steels in ASME standards and recommendations [27,38] is used.

Results

Standard HIC under aqueous H_2S (NACE TM0284)

Hydrogen induced cracking was observed after cross-section of the ×65 steel test coupons after exposure to the standard test environment specified in NACE TM0284). An example of internal crack observed is given in Fig. 6.

The following crack ratio were determined according to NACE TM0284.

- Crack length ratio (CLR): 43.1 ± 12.9%
- Crack thickness ratio (CTR): 5.2 ± 2.0%
- Crack sensitivity ratio (CSR): 1.2 ± 1.0%

According to ISO 15156, a pipeline material is acceptable for sour service if all the following criteria are met: CLR≤15%/CTR≤5%/CSR≤2%. Therefore, the selected alloy is clearly not acceptable for sour service and susceptible to cracking in the presence of H_2S, i.e., in conditions encouraging high hydrogen uptake.

Hydrogen permeation

Fig. 7 compares the hydrogen permeation flux through a 2 mm thick membrane exposed to each of the 3 conditions considered in the work. Several replicates of each condition were performed and there is some scattering in the test results. For instance, the steady state current under dry H_2 varied in the range 0.1–0.3 μA/cm^2, in presence of humidity in the range 0.1–0.5 μA/cm^2 and with humid H_2S reached always several μA/cm^2. Therefore, only a selection of representative experiments was considered in the figure to ease the understanding of the reader.

Nonetheless, the general hydrogen permeation trends are clearly visible after multiple experiments. The rate of hydrogen uptake in wet H_2 is slightly higher than that observed in dry H_2. Contamination with H_2S is even more critical, generating a permeation flux at least one order of

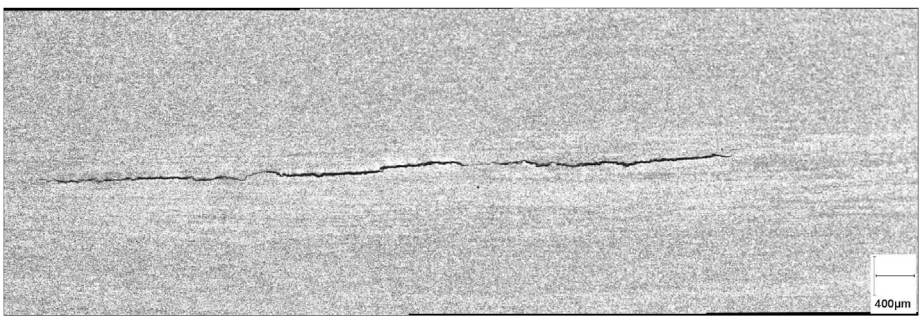

Fig. 6 – Example of HIC cracks observed in the selected ×65 material after standard HIC test.

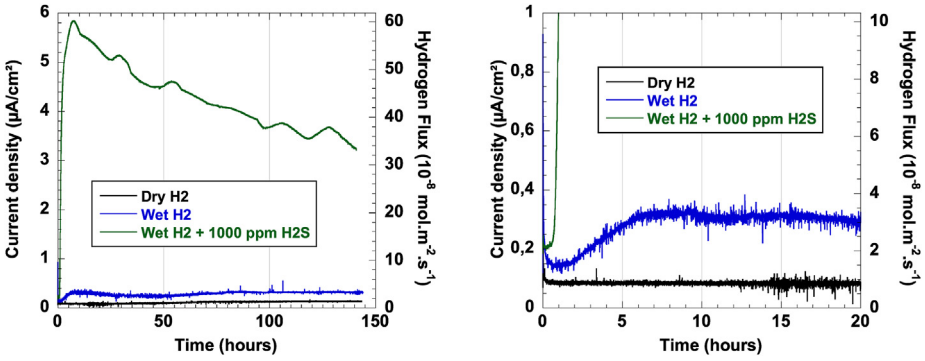

Fig. 7 – Permeation test result in the different test conditions selected. Membrane thickness 2 mm. (a): during 150 h. (b): zoom on the first hours of exposure.

magnitude higher than those measured in both conditions without H_2S. It is also obvious that humid hydrogen is a media that is slightly more severe than dry hydrogen regards the risk of hydrogen embrittlement, and the role of corrosion towards easing hydrogen uptake becomes relevant. The presence of H_2S renders the environment even more critical. In this latter case, we expect that the wet H_2S that is the cause of the hydrogen uptake is mechanistically different (possibly electrochemical charging at the surface from corrosion) instead of only the hydrogen from a gas phase. The contribution of the hydrogen gas is possibly limited.

4 PB tests

To correlate the cracking susceptibility with the hydrogen uptake assessed through permeation experiments, 4 PB tests were conducted in the same environment as those considered for permeation i.e. dry H_2, wet H_2 and wet H_2 contaminated with H_2S. The specimens were loaded at 100% actual yield strength (AYS) of the base material but, in each condition, the base material as well as girth weld were tested. Since the test were conducted on smooth specimens, these tests can be used to address the susceptibility to crack initiation in the test environment considered. None of the tests led to failure, nor to crack initiation. The absence of crack initiation was assessed using ultrasonic checks.

For each test condition, coupons for TDS measurements were also introduced in the autoclaves for post-test TDS measurements and analysis of the hydrogen trapping. The results are displayed in Table 3.

The measured amount of total hydrogen was very low and the diffusible hydrogen therefore even lower (see Table 3). The levels measured are at least one order of magnitude lower than the 1 ppm threshold known as critical to trigger internal cracking according to literature [17,19] and experience. These levels were also those expected for non-stressed specimens, but higher levels are expected if a stress is applied to the material [19], i.e. during the different mechanical tests performed in the hydrogen containing environment.

Slow strain rate tests

Fig. 8 present the plots of the stress versus strain obtained after slow strain rate experiments. The parameters extracted from the test are given in Table 4. The reader is reminded that the tests were performed on a constant extension rate machine which means that no extensometer was used. The elastic modulus and total elongation and all data used without removing the elastic offset are non-consistent. Only the yield strength at 0.2% of elastic offset, the UTS, plastic elongation and reduction of area can be used.

The Table 4 gathers the mechanical parameters obtained from these curves (E_f%) or measured on the specimen (RA%) used to assess the embrittlement of the material during the test. Lower E_f and RA with respect to the control result under 100 bar He indicate some embrittlement. The E_f and RA ratio are the ratio of the plastic elongation and the reduction of

Table 3 – Total hydrogen content measured in the coupons exposed under H_2 pressure during the 4 PB tests.

Test condition	H_{total} (ppb)	
	Base metal	Weld
100 bar dry H_2	0–50	0–50
100 bar humid H_2	20	10–60
100 bar humid H_2 + H_2S	20–50	80–100

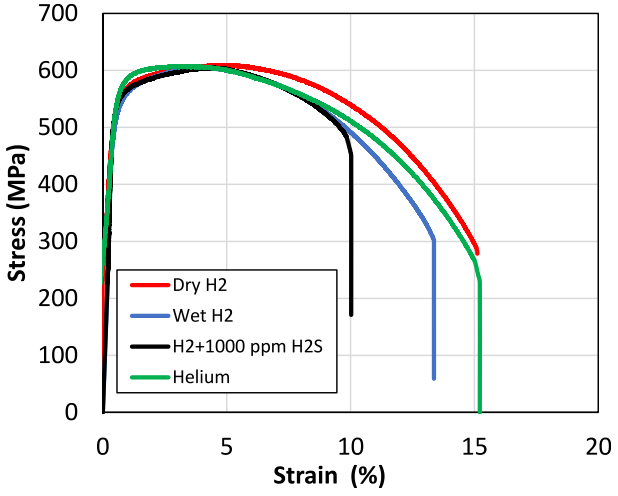

Fig. 8 – Slow strain rate test results in the different conditions selected.

Table 4 – Plastic elongation, reduction of area, elongation ratio and reduction of area ratio determined after each SSR test.

	E_f%	RA%	E_f ratio $E_f(env)/E_f(ref)$	RA ratio $RA(env)/RA(ref)$
Reference – 100 bar Helium	14.9	61	–	
Dry H2 – 100 bar	14.8	58	0.99	0.95
Wet H2 – 100 bar	13.3	53	0.89	0.87
Wet H2 100 bar + 1000 ppm H2S	9.7	26	0.65	0.42

cross-sectional sample area respectively obtained in the H_2 environment compared against the one obtained in the inert reference He test. The higher this ratio, the lower is the relative susceptibility to hydrogen embrittlement.

It is obvious that the embrittlement in dry or wet H_2 is very low, or even negligible since the ductility loss is not higher than 13%. On the contrary, the presence of H_2S dramatically reduced the ductility of the material by at least 35%–58%.

The stress-strain behaviour in the elastic zone is comparable in all 4 cases, and indeed up to UTS. Hydrogen embrittlement is manifested after the initiation of necking. Indeed, the literature shows that the necking produces stress and strain localization and likely ruptures the native oxide layer present at the surface of the specimens that favors localized hydrogen intake and thus embrittlement [54–56]. The effect of hydrogen is stronger on notched specimens, and even more on cracked specimens, because the stress and strain localization are large at the notch root and even larger at the crack tip [57–59]. This recurrent conclusion from the literature is also evident in the rising step load tests for fracture toughness described in the next section.

RSL tests

Fig. 9 presents the monitoring recorded during a RSL test completed under dry H_2 and another under wet H_2 with H_2S contamination. The advantage of the RSL test against the SSRT is HE susceptibility from local hydrogen uptake can be distinguished with greater sensitivity (native oxide rupture/repair during dynamic straining). These data highlight that

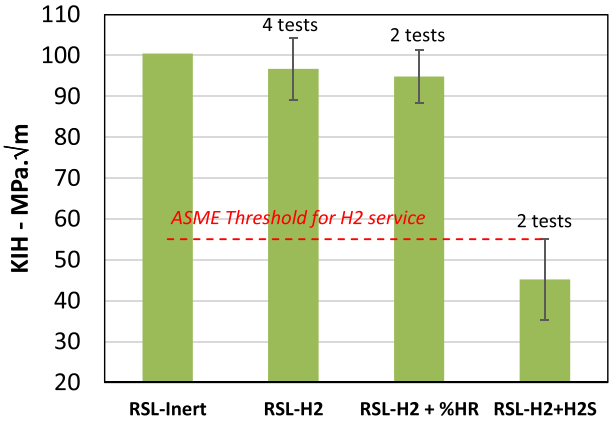

Fig. 10 – K_{IH} measured on ×65 under dry/wet H_2 or under wet H_2 with H_2S contamination.

two different behaviors can be observed depending on the test environment. When loaded under dry hydrogen, Fig. 9 (a), the ECGM monitoring (R/R_0) indicates that the crack does not propagate before the last force step (23.5 kN) at which a sudden failure is observed. The crack propagation mode is therefore critical when the dry hydrogen K_{IH} level is reached. On the contrary, under wet hydrogen with H_2S contamination, the ECGM (R/R_0) highlights that the measured electrical resistance across the material starts increasing at and beyond an applied force of 15 kN while the final failure occurs at about 19 kN. A sub-critical crack propagation initiates therefore before the final failure. Thus, the parameters corresponding to this step when the propagation starts that ought to be employed for the K_{IH} calculation.

Fig. 10 present the K_{IH} values estimated from the RSL experiment conducted in the same environments as those considered for the other test methods. The K_{IH} have been estimated from the evolution of the force versus displacement and up to the threshold at which a propagation start is highlighted through ECGM.

The drop in fracture toughness under 100 bar of dry H_2, is moderate and approximately 5–10%. The drop is quite comparable in the presence of humidity.

With H_2S contamination, the K_{IH} value becomes non-acceptable for hydrogen service according to ASME BPVC as per the fracture mechanics-based design approach.

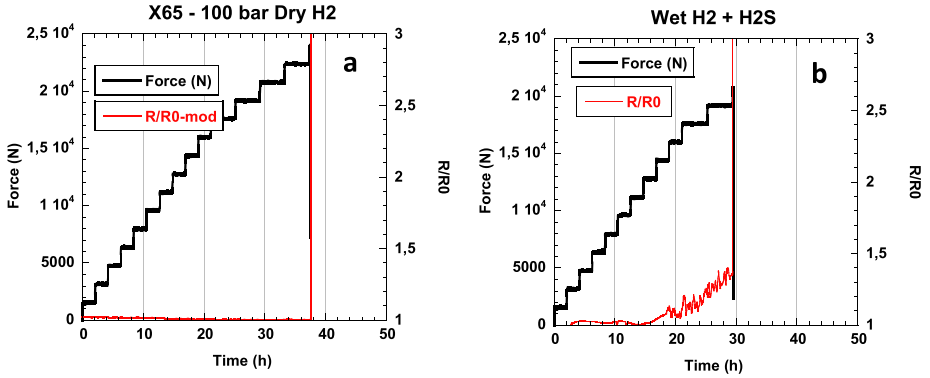

Fig. 9 – Example of monitoring during RSL tests. (a):Test under dry H2. (b) Test under wet H_2 and H_2S contamination.

Indeed, this standard specifies that any grade dedicated to H_2 service shall have a minimum K_{IH} of 50 ksi$\sqrt{in}$ (55 MPa$\sqrt{m}$). With 1000 ppm of H_2S contamination, the K_{IH} measured is only 40 MPa$\sqrt{m}$ corresponding to a drop of more than 60% of the fracture toughness compared to the reference condition.

It is made clear that the results for the inert, dry H_2 and wet H_2 were not obtained in conditions compliant with the geometrical validity checks of the ASTM F1681 as the pipeline wall thickness was too thin, with respect to their K_{IH}. The results should therefore only be considered in relative manner. Only the tests performed with H_2S contamination are compliant with all validity checks and it can therefore be argued that this material is clearly not acceptable in presence of wet H_2S contamination.

The fractographic observations of the CT specimens using SEM are presented in Figs. 11 and 12.

After test under hydrogen, dry, or wet, the fractured surface is very comparable. A brittle crack propagation initiated from the fatigue pre-crack tip but the propagation did not proceed homogeneously along the width of the specimen. The surface is rather clearly brittle in the core of the specimen and ductile on the edges. The brittle fracture extends far in the center of the specimen, with thick plastically deformed edges. This could be due to a preferred diffusion of hydrogen in the central region, where the hydrostatic stress is high, promoting a brittle fracture there. In the example presented, the brittle crack initiated in the center but homogeneous crack initiation along the pre-cracked front were also obtained in test replicates, with reproducible higher brittleness in the center.

After tests in wet hydrogen with H_2S contamination, the fractured surface is completely different. The expected homogeneous transgranular crack propagation is visible, which in this case advanced until the remaining material ligament was too short to sustain the tensile stress applied, thus leading to a final ductile fracture. Here, no deep extension of the brittle zone is noted within the central part of the ruptured specimen, as previously observed in the tests without H_2S. This could be due to a smaller sensitivity of hydrogen diffusion to hydrostatic stress, or more simply, to the relatively lower value of the hydrostatic stress, as the fracture load was much lower than for the other tests.

Despite the rather low sensitivity of the steel to hydrogen embrittlement under 100 bar of dry or wet hydrogen gas according to RSL tests, the fractographic analyses revealed brittle failure, at least in the mid-section of the CT samples. According to the fracture mechanics theory, it could be assumed that this area was closed to plane strain conditions, resulting in higher stress triaxiality [60]. In this case, the diffusion of hydrogen to the mid-section would be favored to

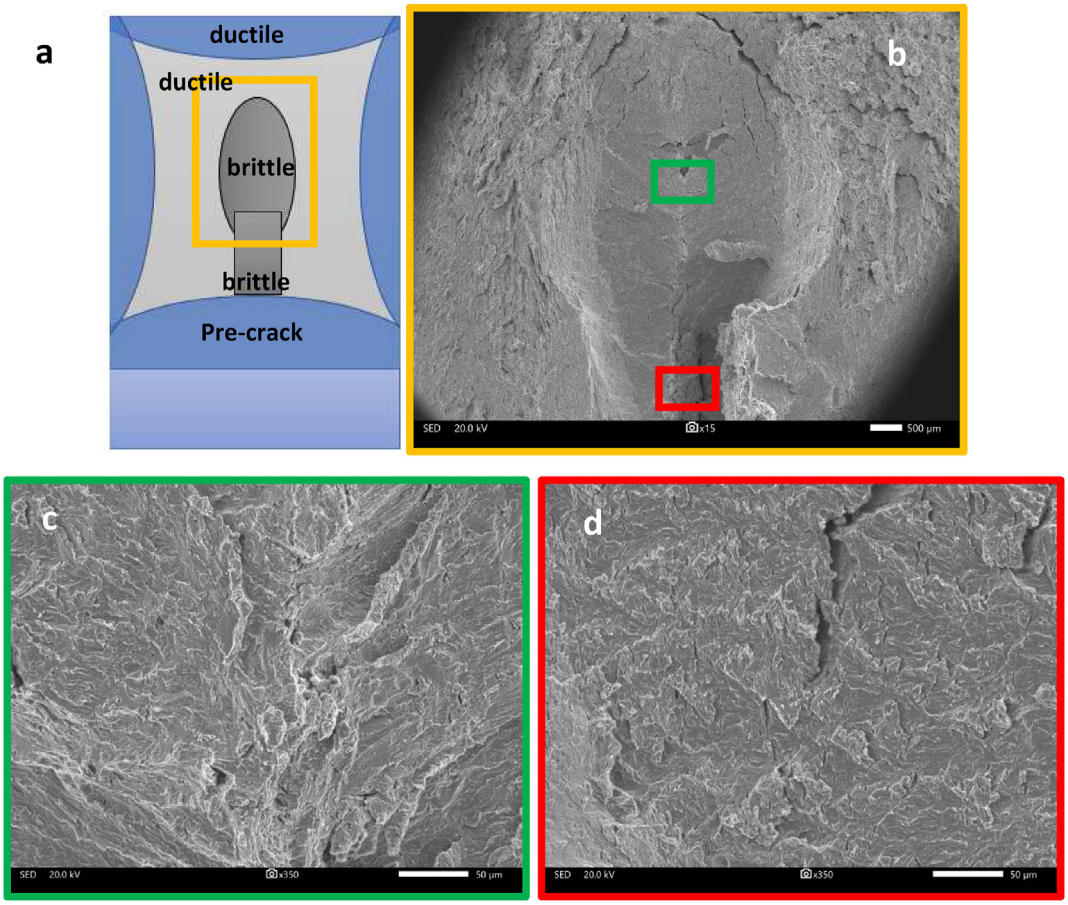

Fig. 11 – Fractographic observations of the CT specimen tested under 100 bar of dry H_2 with RSL. (a): cartoon of fractured surface observations. (b-c-d): SEM observations of the areas highlighted by rectangles on the figures(a) and (b) showing how the brittle fracture propagated in the middle of the specimen and ductile failure on the edges.

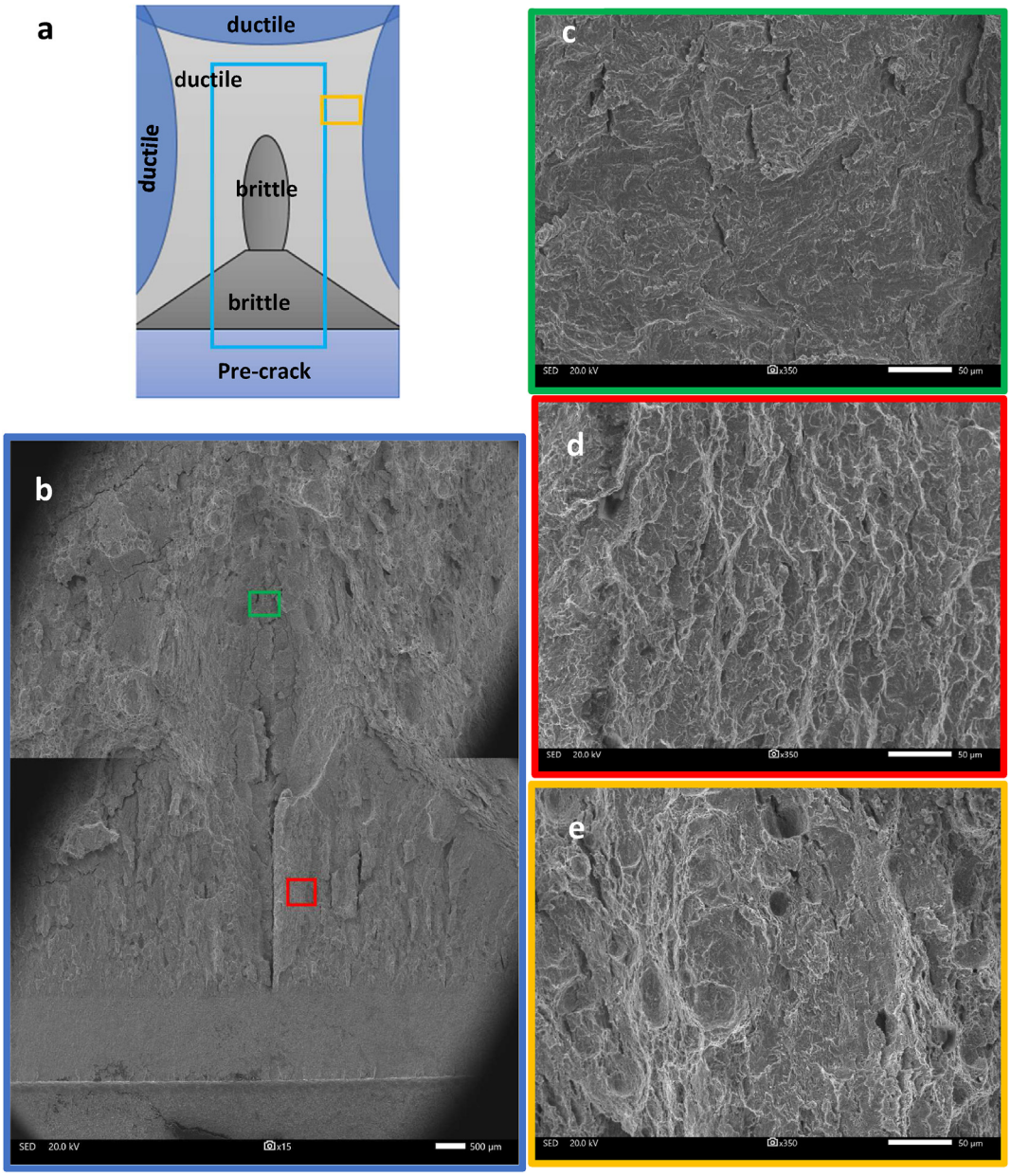

Fig. 12 – Fractographic observations of the CT specimen tested under 100 bar of wet $H_2 + H_2S$ with RSL. (a) cartoon of what is observed on the fractured surface. (b-c-d): SEM observations of the areas highlighted by rectangles on the figures (b) and (c) showing an initial brittle propagation crack followed by a ductile final fracture. (d) evidence of MVC on the non-pre-cracked edge suggesting ductile failure at this site.

this high hydrostatic stresses, resulting in higher local hydrogen concentration [61, 62]. From electrical monitoring, no sub-critical cracking was measured. On this basis, the crack growth rate must have been quite high on the last load increment. Thus, the crack could have first propagated from the pre-crack at the location of the highest hydrogen activity, which was the mid-section of the sample, followed by rapid expansion through the entire section at the application of the higher load.

For the specimens tested with and without H_2S addition (Figs. 11 and 12) an oval-shaped brittle area can been seen some millimeters ahead the tip of the pre-crack. The hydrostatic stress concentration ahead a crack tip is suggested to be confined within the first 500 µm [64]. Thus, this pattern could not be explained by local hydrogen oversaturation prior to cracking due to the stress triaxiality. An effect of elemental macro-segregation cannot be ruled out considering the sampling location of the CT at mid-wall thickness of the pipelines.

Further analyses of the fracture surfaces would be required to understand the cracking scenario and explain such brittle areas. It was indeed unexpected to observe brittle facets associated with high K_{IH} levels. Analysis using statistical fractography may elucidate this result.

Discussion

According to the hydrogen permeation experiments, it is obvious that the presence of humidity tends to increase the severity of the pressurized hydrogen environment leading to an increased hydrogen uptake if compared against the dry hydrogen atmosphere. On the contrary, the presence of a H_2S contamination as low as 1000 ppm, in humid pressurized H_2, dramatically increases the hydrogen flux by at least one order of magnitude. No experiment was conducted with H_2S in dry environment, since it is well known that the effect of this gas as a hydrogen entry promoter exists in aqueous environments through a catalytic electrochemical process. Although no stress was applied on the membrane during testing, these permeation tests were used to correlate the hydrogen flux in the material exposed to a given environment to the crack susceptibility.

Regarding the susceptibility to crack initiation using SSR tests, it was highlighted that the effect of dry or wet hydrogen on the plastic elongation and reduction of area of the specimens is very limited whereas the impact is higher when some H_2S is present in the gas phase. However, no significant difference was observed between the different media considered after constant strain tests using 4 PB. Regardless of the environment, none of the 4 PB specimens failed and no HIC initiation was visible after ultrasonic inspection.

On the contrary, the susceptibility to propagation of a pre-existing crack seems well correlated to the intensity of the hydrogen uptake: the higher the permeation flux and the lower the K_{IH} determined using RSL test. From these RSL results, the impact of hydrogen gas, dry or wet, on the crack propagation up to 100 bar seems somewhat limited with respect to the control data under 100 bar He. In any case, the measured K_{IH} are largely higher than the threshold limits specified in ASME BPVC for hydrogen service.

On the contrary, the fracture toughness of the material exposed to 100 bar of humid hydrogen contaminated with 1000 ppm of H_2S is further decreased and becomes unacceptable for hydrogen service according to ASME requirements [26,27]. This effect is attributed to sour hydrogen uptake, well known to generate sour cracking, and not to the presence of hydrogen gas.

Conclusion

To address the risk of embrittlement in conditions representative of hydrogen storage and transport, this study was conducted on an ×65 steel low carbon steel grade susceptible to hydrogen assisted cracking. Three different pressurized environments were considered, namely dry hydrogen, wet hydrogen, and wet hydrogen with H_2S contamination to levels that representative of higher extreme quantities that may be present in biogas.

The main conclusions are.

- According to permeation experiments, the presence of humidity slightly increases the severity of the environment but H_2S contamination increases this severity by at least one order of magnitude. This increase is attributed to H_2S only (sour charging), not to any effect of hydrogen and should therefore also occur with only biogas if humidity is present.
- Dry hydrogen under 100 bar only slightly affects the resistance of the material to hydrogen assisted crack initiation.
- On the contrary, the modification of the environment strongly affects fracture toughness. The material remains acceptable for service as per ASME BPVC in absence of H_2S but, with traces of this contaminant in a humid atmosphere, the fracture toughness dramatically decreases down to unacceptable levels.

Declaration of competing interest

The authors declare that they have no known competing financial interests or personal relationships that could have appeared to influence the work reported in this paper.

REFERENCES

[1] Hydrogen RoadMap Europe « A sustainable pathway for the European energy transition ». FCH2JU; 2019. web link : https://www.fch.europa.eu/sites/default/files/Hydrogen%20Roadmap%20Europe_Report.pdf.
[2] Chapman A, Itaoka K, Hirose K, Davidson FT, Nagasawa K, Lloyd AC, Webber ME, Kurban Z, Managi S, Tamaki T, Lewis MC, Hebner RE, Fujii Y. A review of four case studies assessing the potential for hydrogen penetration of the future energy system. Int J Hydrogen Energy 2019;44:6371–82.
[3] Pugazhendhi A, Chen W-H. Hydrogen energy technology for future. Int J Hydrogen Energy 2022;47:37153.
[4] Ohaeri E, Eduok U, Szpunar J. Hydrogen related degradation in pipeline steel: a review. Int J Hydrogen Energy 2018;43:14584–617.
[5] Capelle J, Gilbert J, Dmytrakh I, Pluvinage G. Sensitivity of pipelines with steel API X52 to hydrogen embrittlement. Int J Hydrogen Energy 2008;33:7630–41.
[6] Zhou D, Li T, Huang D, Wu Y, Huang Z, Xiao W, Wang Q, Wang X. The experiment study to assess the impact of hydrogen blended natural gas on the tensile properties and damage mechanism of X80 pipeline steel. Int J Hydrogen Energy 2021;46:7402–14.
[7] Wang H, Tong Z, Zhou G, Zhang C, Zhou H, Wang Y, Zheng W. Research and demonstration on hydrogen compatibility of pipelines: a review of current status and challenges. Int J Hydrogen Energy 2022;47:28585–604.
[8] Eames I, Austin M, Wojcik A. Injection of gaseous hydrogen into a natural gas pipeline. Int J Hydrogen Energy 2022;47:25745–54.
[9] Wu X, Zhang H, Yang M, Jia W, Qiu Y, Lan L. From the perspective of new technology of blending hydrogen into natural gas pipelines transmission: mechanism, experimental study, and suggestions for further work of hydrogen embrittlement in high-strength pipeline steels. Int J Hydrogen Energy 2022;47:8071–90.
[10] Report "Development of business Cases for fuel Cells and hydrogen Applications for European Regions and cities" commissioned by the fuel cells and hydrogen 2 joint undertaking (FCH2JU), N°FCH/OP/contract 180, Reference Number FCH JU2017 D4259.

[11] Huang S, Hui H. Predictive environmental hydrogen embrittlement on fracture toughness of commercial ferritic steels with hydrogen-modified fracture strain model. Int J Hydrogen Energy 2022;47:10777–87.
[12] Wang C, Zhang J, Liu C, Hu Q, Zhang R, Xu X, Yang H, Ning Y, Li Y. Study on hydrogen embrittlement susceptibility of X80 steel through in-situ gaseous hydrogen permeation and slow strain rate tensile tests. Int J Hydrogen Energy 2022;48:243–56.
[13] Jack TA, Pourazizi R, Ohaeri E, Szpunar J, Zhang J, Qu J. Investigation of the hydrogen induced cracking behaviour of API 5L X65 pipeline steel. Int J Hydrogen Energy 2020;45:17671–84.
[14] Zivar D, Kumar S, Foroozesh J. Underground hydrogen storage: a comprehensive review. Int J Hydrogen Energy 2021;46:23436–62.
[15] Sambo C, Dudun A, Samuel SA, Esenenjor P, Muhammed NS, Haq B. A review on worldwide underground hydrogen storage operating and potential fields. Int J Hydrogen Energy 2022;47:22840–80.
[16] Rasi S, Veijanen A, Rintala J. Trace compounds of biogas from different biogas production plants. Energy 2007;32:1375–80.
[17] J. Kittel et al. "Hydrogen induced cracking (HIC) – Laboratory testing assessment of low alloy steel linepipe" NACE Corrosion Conference 2008 paper 08110.
[18] Nagao A, et al. Hydrogen-enhanced-plasticity mediated decohesion for hydrogen-induced intergranular and quasi-cleavage fracture of lath martensitic steels. J. mech. phy. solids 2018;112:403–30.
[19] Capelle J. Evaluation of electrochemical hydrogen absorption in welded pipe with steel API X52. Int. J. of Hydrogen energy 2013;38:14356–63.
[20] Kotrechko SO, Krasowsky AY, Meshkov YY, Torop VM. Effect of long-term service on the tensile properties and capability of pipeline steel 17GS to resist cleavage fracture. Int.J. Pressure Vessels and Piping 2004;81(4):337–44.
[21] Nykyforchyn H, Lunarska E, Tsyrulnyk O, Nikiforov K, Gabetta G. Effect of the long-term service of the gas pipeline on the properties of the ferrite–pearlite steel. Mater Corros 2009;60(9):716–25.
[22] Zvirko O, Gabetta G, Tsyrulnyk O, Kret N. Assessment of in-service degradation of gas pipeline steel taking into account susceptibility to stress corrosion cracking" Procedia structural integrity, vol. 16; 2019. p. 121–5.
[23] Briottet L, Moro I, Lemoine P. Quantifying the hydrogen embrittlement of pipeline steels for safety considerations. Int J Hydrogen Energy 2012;37:17616–23.
[24] Michler T, Naumann J. Microstructural aspects upon hydrogen environment embrittlement of various bcc steels. Int. J. Hydrogen Energy 2010;35:821–32.
[25] Moro I, Briottet L, Lemoine P, Andrieu E, Blanc C, Odemer G. Hydrogen embrittlement susceptibility of high strength steel X80. Mater Sci Eng 2010;527(27–28):7252–60.
[26] ASME Boiler and Pressure Vessel code (BPVC) – 2019 – section VIII – rules for construction of pressure vessels.
[27] Asme B31.12-2011 – hydrogen piping and pipelines – ASME code for pressure piping, B31.
[28] San Marchi C, Somerday BP, Nibur KA. Development of standards for evaluating materials compatibility with high-pressure gaseous hydrogen. In: International conference on hydrogen safety; 2013.
[29] Nobuyuki I, Junji S, Daichi I, Hiroshi O, Yoshihiro N. Hydrogen effect on linepipe steel and material compatibility to a high pressure hydrogen pipeline" International. Journal of Offshore an Polare Engineering 2022;32(4):448–56.
[30] San Marchi C, Somerday BP. Sandia report sand2012-7321, technical reference for hydrogen compatibility of materials. Alburquerque, NM: Sandia National Laboratories; 2012.
[31] Nastich SY, Lopatkin VA. Effect of hydrogen gas on mechanical properties of pipe metal of main gas pipelines. Metallurgist 2022;66(5–6):625–38.
[32] Genchev G, Mentz J, Brauer H, Kalwa C, Muthmann E, Ratke D. Safety considerations for the transport of hydrogen gas in line pipes and induction of bent pipes. In: Biennal International pipeline conference. vol. 1; 2022. paper v001t08a004 - Calgary.
[33] Thebault F, Designolle V, Delattre L. Stress cracking and fatigue resistance of seamless pipes fo hydrogen storage and transport applications. In: AMPP conference; 2023. paper 19050.
[34] Thebault F, Designolle V. Hydrogen stress cracking resistance of seamless pipes for hydrogen storage and transport applications. In: International Petroleum Exhibition and Conference; 2022 [Abu Dhabi].
[35] G. Benoit, D. Bertheay, G. Henaff, L. Alvarez, "Crack growth resistance of actual pipe weldments exposed to a high pressure mixture of hydrogen and natural gas" ASME 2021 Pressure Vessels and Piping Conference. Paper V004T06A051.
[36] Martin LM, Connoly M, Buck NZ, Bradley EP, Lauria D, Slifka AJ. Evaluating a natural gas pipeline steel for blended hydrogen service. J Nat Gas Sci Eng 2022;101.
[37] Peral LB, Zafra A, Rodriguez C, Belzunce J. Evaluation of strength and fracture toughness of ferritic high strength steels under hydrogen environments" Procedia. Structural Integrity 2017;5:1275–82.
[38] Briottet L, Moroa I, Escota M, Furtado J, Bortot P, Tamponi GM, Solin J, Odemer G, Blanc C, Andrieu E. Fatigue crack initiation and growth in a CrMo steel under hydrogen pressure" International. J. Hydrogen Energy 2015;40:17021–30.
[39] Sun Z, Benoit G, Moriconi C, Hamon F, Halm D, Hamon F, Hénaff G. Fatigue crack propagation under gaseous hydrogen in a precipitation-hardened martensitic stainless steel. Int J Hydrogen Energy 2011;36:8641–4.
[40] Dadfarnia M, Sofronis P, Brouwer J, Sosa S. Assessment of resistance to fatigue crack growth of natural gas line pipe steels carrying gas mixed with hydrogen. Int. J. Hydrogen Energy 2019;44:10808–22.
[41] Wang S, Nagao A, Sofronis P, Robertson IM. Hydrogen-modified dislocation structures in a cyclically deformed ferritic-pearlitic low carbon steel. Acta Mater 2018;144:164–76.
[42] Cialone HJ, Holbrook JH. Effects of gaseous hydrogen on fatigue crack growth in pipeline steel. Met. Trans. A 1985;16A(1):115–22.
[43] Nibur KA, Somerday BP, Marchi CS, Foulk JW, Dadfarnia M, Sofronis P. The relationship between crack-tip strain and subcritical cracking thresholds for steels in high-pressure hydrogen gas. Met. Trans.A 2013;44A:248–69.
[44] Yoshikawa M, Matsuo T, Tsutsumi N, Matsunaga H. Effects of hydrogen gas pressire and test frequency on fatigue crack growth properties of low carbon steel in 0.1-90 MPa hydrogen gas. Trans. of the JSME 2014;80(817):1–16.
[45] Briottet L, Moro I, Escot M, Furtado J, Bortot P. Fatigue crack initiation and growth in a CrMo steel under hydrogen pressure. Int. J. Hydrogen Energy 2015;40:17021–30.
[46] Ronevich JA, Somerday BP. Effects of microstructure banding on hydrogen assisted fatigue crack growth in X65 pipeline steels. Int. J. of fatigue 2016;82:497–504.
[47] U. B. Baek U.B. H. M. Lee, S. W. Baek. "Hydrogen embrittlement for X-70 pipeline steel in high pressure hydrogen gas" – Proceedings of the ASME 2015 Pressure Vessels and Piping Conference Boston, MA USA – Paper PVP2015-45475.
[48] Florisson - presentation NaturalHy O. Assessing the potential of the existing natural network for hydrogen delivery - GERG Academic Network Event. 2010. Brussels 4th June.

[49] Preparing for the hydrogen economy by using the existing natural gas system as a catalyst (NATURALHY) – may 2004-Oct 2009 – European funding #502661 – program "FP6 - SUSTDEV-1.2.2 - new technologies for energy carriers – hydrogen".
[50] Specification API 5L – specification of line pipe –. October 2008.
[51] NACE TM 0284. Evaluation of pipeline and pressure vessel steels for resistance to hydrogen induced cracking. 2016.
[52] Devanathan MAV, Stachurski Z. The mechanism of hydrogen evolution on iron in acid solutions by determination of permeation rates. J Electrochem Soc 1964;111:619–23.
[53] I. Moro – Fragilisation par l'hydrogène gazeux d'un acier ferrito-perlitique de grade API X80 – PhD thesis defended the 13th of november 2009 – Toulouse university, France.
[54] Miresmaeili R, Ogino M, Nakagawa T, Kanayama H. A coupled elasto-plastic transient hydrogen diffusion analysis to simulate the onset of necking in tension by using the finite element method. Int J Hydrogen Energy 2010;35:1506–14.
[55] Guedes D, Oudriss A, Frappart S, et al. The influence of hydrostatic stress states on the hydrogen solubility in martensitic steels. Scripta Mater 2014;84–85:23–6.
[56] Kan B, Wu W, Yang Z, Li J. Stress-induced hydrogen redistribution and corresponding fracture behavior of Q960E steel et different hydrogen content. Materials Sci. Eng Anal 2020;775:138963.
[57] Cui TC, Liu PF, Gu CH. Finite element analysis of hydrogen diffusion/plasticity coupled behaviors of low-allow ferritic steel at large strain. Int J Hydrogen Energy 2017;42:20324–35.
[58] Martinez-Paneda EM, Golahmar A, Niordson CF. A phase field formulation for hydrogen assisted cracking, Comput. Methods Appl. Mech. Engrg 2018;342:742–61.
[59] Gonzales P, Cicero S, Arroyo B, Alvarez JA. A theory of critical distances based methodology for the analysis of environmentally assisted cracking in steels. Eng Fract Mech 2019;214:134–48.
[60] Chen CR, Kolednik O, Heerens J, Fischer FD. Three-dimensional modeling of ductile crack growth: cohesive zone parameters and crack tip triaxiality. Eng Fract Mech 2005;72(13):2072–94.
[61] Sofronis P, McMeeking RM. Numerical analysis of hydrogen transport near a blunting crack tip. J Mech Phys Solid 1989;37(3):317–50.
[62] Li Y, Zhang K, Lu D, Zeng B. Hydrogen-assisted brittle fracture behavior of low alloy 30CrMo steel based on the combination of experimental and numerical analyses. Materials 2021;14:3711.